Geometric Optics with Uniform Asymptotic Physical Optics for Ray Tracing of Compound GRIN Lens Systems

Wei Wang[#1], Jonathan Chisum[#2]
[#]Department of Electrical Engineering, University of Notre Dame, Notre Dame, IN, USA
[1]wwang23@nd.edu, [2]jchisum@nd.edu,

***Abstract*— In this paper, a compound Gradient-Refractive Index (GRIN) lens simulation method using hybrid Geometrical Optics and Uniform Asymptotic Physical Optics is proposed. The ray distributions of the compound lens structure are analyzed and seven major regions are described in detail with an example showing diffracted fields of both lenses. To improve the accuracy, a ray tracing design flowchart is given with an iterative ray-launching procedure to ensure proper ray spacing in the radiating aperture. An impedance-matched compound GRIN lens structure is simulated with the proposed numerical method (requiring only 2.5 minutes) and compared with a full-wave simulator (requiring about 3 hours). The hybrid ray tracing has a gain error of 0.2 dB, a sidelobe level error of 4.7 dB and a 3dB beamwidth error of 0.1°.**

***Keywords*— Gradient Refractive Index, compound lens, ray tracing, diffraction.**

I. Introduction

Recently, Gradient-Refractive Index (GRIN) lenses have been investigated as low-cost and low-power beam scanning antennas for millimeter wave radar[1] and wireless communications[2][3][4][5]. Typical GRIN lenses are ϕ-symmetric cylinders with one-dimensional permittivity profiles. These simplified lenses are amenable to geometric optics ray tracing and even closed-form designs which yield high gain and optimal broadside aperture efficiency[2][4]. However, these design methods are only strictly valid for broadside beams—for scanned beams the collimation degrades. Some lens designs incorporate impedance matching layers to the lens surfaces to improve transmission efficiency[3][6] but the matching layers require a two-dimensional permittivity profile, resulting in ray trajectories which are not tractable in closed-form expressions. In addition to using matching layers to increase bandwidth, some designs include secondary lenses to improve beam scanning performance. For example, double-lens systems like the discrete feed corrective lenslets (FCLs)[7] and the continuous focal lens[8] have been reported with a wide-angle beam scan capability with low scan loss. Compared with the single lens system, compound lenses squint the feed pattern toward the aperture lens such that spillover efficiency is improved and scan loss is reduced.

Both the matching layers for bandwidth enhancement and compound lens systems for wide-angle, low-scan loss performance further exacerbate the difficulty of accurately designing and even simulating the lenses in a time-efficient manner. Since no closed-form expression exists for the design of matched and compound lens systems, it is necessary to optimize the permittivity profiles. Full-wave simulation of GRIN lenses is accurate but time-consuming and memory-intensive making it difficult or impractical to optimize the permittivity profile with global optimization like Particle Swarm Optimization. Compound lenses aggravate the issue by doubling the number of free parameters in the lens design and increasing simulation time and memory. As an alternative solution, Geometrical Optics (GO) ray tracing utilizes a collection of light rays to represent electromagnetic wave propagation and attains the lens aperture fields and far-field pattern[9]. By adding diffraction analysis[10], a hybrid ray tracing tool involving GO and Uniform Asymptotic Physical Optics(UAPO) can simulate practical GRIN lenses as reported in [11]. While maintaining high accuracy, this method takes only one minute for each lens simulation enabling iterative global optimization of lens parameters. However, to date these methods are not suitable for compound lens systems.

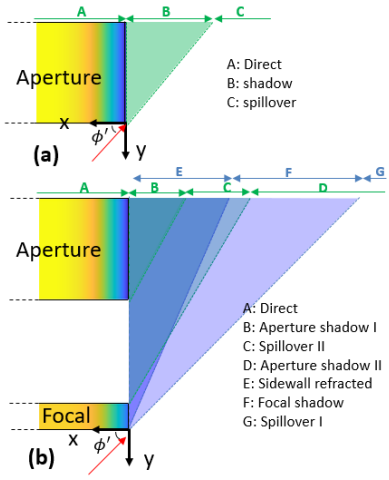

Fig. 1. (a) Single lens aperture ray distribution. (b) Compound lens ray distribution. Green shows regions related to the aperture lens and blue shows regions related to the focal lens.

This work proposes a novel method for simulating compound lenses using a hybrid GO ray tracing with diffraction. First, the unique distribution of rays in compound lens systems is discussed. In light of the unique ray trajectories, a general method for aperture field calculation is proposed and summarized with a flowchart. To address the extreme ray trajectories in compound systems an iterative ray-shooting method is proposed which increases ray density in regions of poor ray coverage. For regions with little or no ray coverage diffraction fields from both lenses are computed. To

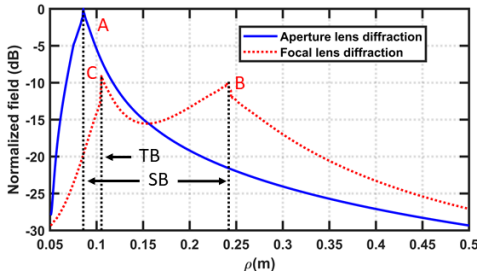

Fig. 2. Electrical field magnitude comparison between the focal lens diffracted fields and the aperture lens diffracted fields. The values are recorded at the aperture lens upper bound plane. "TB" represents the transmission boundary caused by refraction and "SB" represents the shadow boundary.

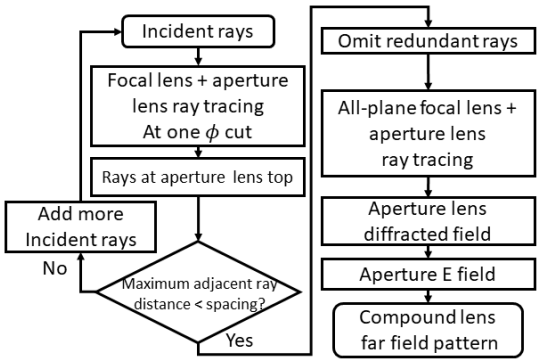

Fig. 3. Compound lens ray tracing design flowchart.

demonstrate the proposed method a matched, the compound lens is simulated and compared with full-wave simulation.

II. Theory

The geometry of the compound lens system under consideration is described as follows. Both GRIN lenses are ϕ-symmetric with flat upper and lower boundaries. The refractive index distribution $n(\rho)$ can be characterized as a monotonic fourth-order polynomial where the minimum index of refraction (occurring at the sidewall, $\rho = D/2$) is $n\left(\rho = \frac{D}{2}\right) > 1$. The feed is modeled as a point source launching a spherical wave polarized along the y-axis and with amplitude distribution extracted from a WR-28 10 dBi horn antenna full-wave simulation at 40 GHz. The focal lens (closest to the feed elements) should be placed in the far-field of the given feed, at least 16.9 mm away.

Compound lens ray distribution: Although the hybrid ray tracing for a single practical lens design has been investigated in [11], the compound lens structure complicates the ray trajectories, making the ray tracing more challenging. In Fig. 1(a), a single lens aperture ray distribution is shown, with three regions defined based upon the presence or absence of various classes of rays. Region A is the "Direct" region, where the rays travel through the lens and into the radiating aperture. Region C is the "Spillover Region", where aperture rays only travel in the air. Region B is called the "Shadow Region", which is caused by internal reflections from the lens side wall, causing no rays to land in this region. Therefore the fields in Region B can only be solved by more sophisticated theories such as diffraction theory. In contrast, Fig. 1(b) shows the compound lens structure which generates two types of shadow regions (due to two lens sidewalls), and an extra spillover region due to the air gap between the two lenses. Despite lying outside the lens aperture, these regions still contribute to the radiation pattern and greatly influence the hybrid ray tracing accuracy, therefore it is necessary to investigate a general compound lens ray tracing distribution.

Overall, there are seven regions which should be considered. Region A to Region D is mainly influenced by the air gap and the aperture lens. Region A shows the direct rays that travel through both lenses. Region B represents a shadow region near the aperture lens sidewall. Similar to [11], we assume the aperture lens side wall results in total internal reflection and therefore the boundary between Region A and B is precisely the lens sidewall. In the single-lens case, the incident field at the lens sidewall can be analytically derived using the feed pattern and F/D. However, in the compound lens system, the aperture lens is not directly illuminated by the feed. Therefore, the incident ray to the aperture lens edge is found to be the focal lens exit ray that lands closest to the aperture lens edge, and the incident angle of this edge ray also determines the shadow region boundary. Region C is a secondary spillover region including rays that travel through the focal lens upper boundary but circumvent the aperture lens. The span of this spillover is affected by the focal lens permittivity profile, and beyond the spillover, Region D represents another shadow region whose fields can be found from aperture lens diffraction. The boundary between Region C and D is also affected by the focal lens permittivity profile.

Compared with the aforementioned four regions, Region E to Region G are mainly influenced by the focal lens. Unlike the aperture lens, the effective F/D ratio for the focal lens (relative to the feed) is smaller than the F/D of the aperture lens resulting in larger oblique incident angles at the lens edge. As a result, Region E contains refracted rays traveling *through* the focal lens sidewall. Because refracted ray angles vary rapidly at a narrow sidewall region, rays should be launched with a higher density at the lens edge than at the lens center to capture sufficient ray density in the radiating aperture (See discussion on ray tracing procedures). Region F is the focal lens shadow region with the boundary angle between Region E and F determined by:

$$\phi_{EF} = \text{acos}(\sqrt{\epsilon_r - \cos^2\phi'}) - \frac{\pi}{2}, \phi_{EF} \in [\pi, \frac{3}{2}\pi] \quad (1)$$

where ϕ' is the ray incident angle to the lens edge and ϵ_r is the permittivity at the lens edge. Finally, Region G is the focal lens spillover region.

We note that depending on the focal lens properties, Region B to D may overlap with Region E to G, and when they overlap, electrical fields at each region should be calculated separately and analyzed separately to either determine a dominant field or add all fields together as a vector sum. For example, one would assume the focal lens diffraction is trivial (compared to the aperture lens diffraction) due to the extra

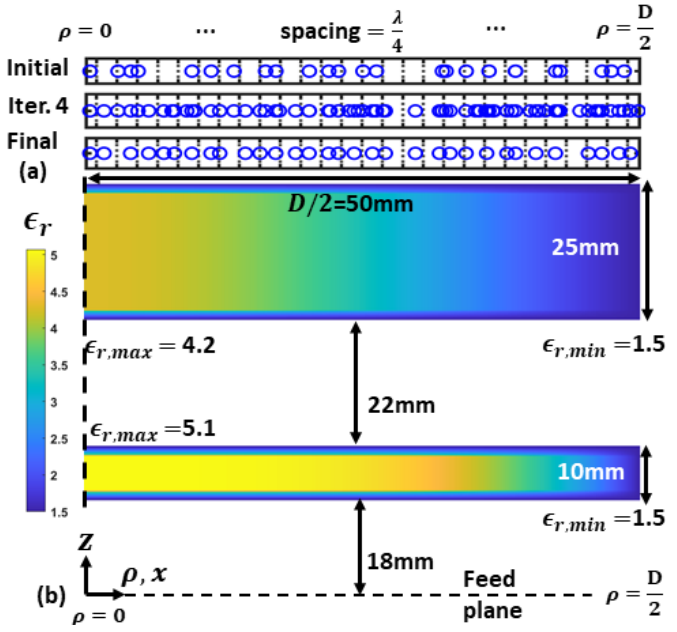

Fig. 4. (a)Ray occupancy with respect to the desired ray spacing from $\rho = 0$ to $\rho = D/2$ at the aperture lens upper surface. The desired spacing is shown as grids, and if an aperture ray (blue dots) is positioned within a unit, the electrical fields of the unit area is sampled by the ray. (b)The dimension of the proposed compound lens dimension for ray tracing demonstration from $\rho = 0$ to $\rho = D/2$.

distance from the diffraction point to the radiating aperture. However, its contribution can be significant in certain regions compared to the aperture lens diffraction. Figure 2 shows the comparison of the normalized diffracted fields due to focal lens diffraction (dashed, red) and aperture lens diffraction (solid, blue). The compound lens setup of this simulation will be shown in Section III. There are three peaks in total: peak A and peak B represent boundaries between the shadow region and the spillover region. Peak C shows the boundary between the refracted ray region and the shadow region, which can be derived by (1). Therefore, Region B is dominated by aperture lens diffraction, and diffraction in regions with $\rho >$0.1 m (e.g., Region D) is dominated by focal lens diffraction, which is different from the assumption.

Compound lens ray tracing procedure: Given the complexity of the compound lens ray tracing and the fact that rays can be directed to extreme angles between the many lens surfaces, it is necessary to capture sufficient rays in the lens aperture (or radiating) plane. In [9], [11] the rule of thumb was to launch rays with $\lambda/2$ spacing at the lower lens boundary. However, with the existence of Region C, some rays following the old procedure become spillover rays such that the $\lambda/2$ spacing cannot be achieved at the aperture lens upper boundary. Also, depending on the lens structure complexity, finer sampling might be implemented to improve accuracy. Therefore, Figure 3 proposes a ray tracing procedure for compound lenses which ensures the radiating aperture plane is critically sampled (or better) with rays.

At first, the incident ray angles from the feed are determined in a single ϕ cut without calculating electrical

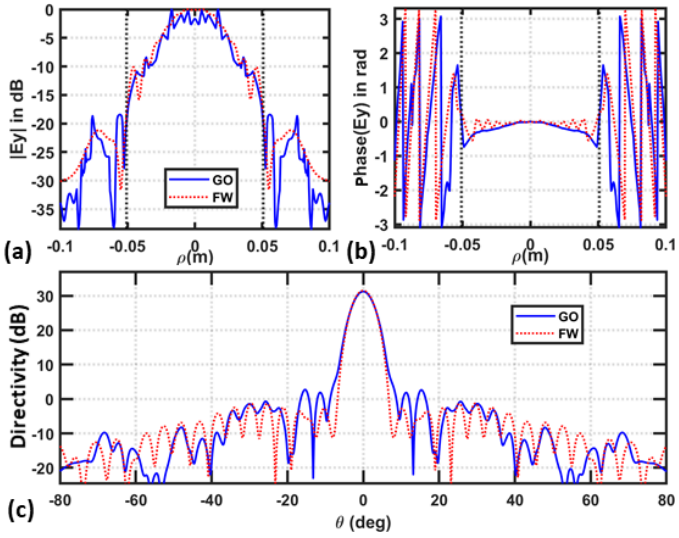

Fig. 5. (a) Aperture $|E_y|$. (b) Aperture $\angle E_y$. (c) Far-field pattern.

fields—this saves computation time. After ray tracing through both the focal lens and the aperture lens, ray density in Region A is evaluated and if the minimal ray distribution does not meet the desired density, more rays are launched between existing incident rays to fill the vacancy. Note there will be an upper limit for the iteration because some lens permittivity will generate regions that rays can never reach. After the upper limit is achieved or the minimal ray distance is qualified, redundant rays will be omitted to save simulations time. After determining the incident rays at one ϕ cut, a complete two-lens ray trace will be implemented with electrical field calculation. After determining electrical fields associated with rays, analytical diffracted fields are calculated from focal lens diffraction and aperture lens diffraction and the resulting diffraction fields are added together for far-field pattern evaluation. Note here we only mention rays in Region A (those rays which pass through both the focal lens and the aperture lens) but the same ray spacing requirement should be enforced in all other regions of the aperture plane.

Figure 4(a) demonstrates the proposed ray-shooting procedure where markers in each stacked plot correspond to rays in a single ϕ cut in the radiating aperture. A finer spacing of $\lambda/4$ at 40 GHz is used as the sampling criterion. The "Initial" ray trace results in multiple rays in a single $\lambda/4$ region while other regions have no rays. Iterative ray-launching beings to fill in each $\lambda/4$ region (see "Iter. 4"). Due to the unpredictable nature of the ray trace result, some rays are ultimately pruned to omit redundant rays. The "Final" iteration contains only one ray in each $\lambda/4$ region which yields sufficient sampling density while not computing more than is necessary.

III. Demonstration & Conclusion

To demonstrate the proposed hybrid ray tracing, Fig. 4(b) shows the dimension of a compound lens structure from the centerline ($\rho = 0$) to the edge ($\rho = D/2$). Although the lens design process is beyond the scope of this paper,

Table 1. Simulation results

Method	Lens performance			Time
	Directivity (dB)	SLL (dB)	3dB BW (°)	
FW	31.4	34.1	4.0	3h
GU	31.2	29.4	4.1	2.5min

the lens model is derived using the iterative design method described in [6]. The aperture lens radial permittivity profile is $\epsilon_r(\rho) = 230053\rho^4 - 1667.4\rho^2 + 4.27$ and the focal lens profile is $\epsilon_r(\rho) = -520235\rho^4 - 39.01\rho^2 + 5.06$. Klopfenstein tapers are included on the top and bottom surfaces of both lenses for impedance matching. Figure 5(a)-(c) compares the results from full-wave FDTD (Empire XPU) and the proposed compound-lens GO+UAPO simulator. In general, the GO+UAPO y-polarized aperture fields (5(a) and (b)) and far-field radiation patterns (Fig. 5(c)) agree very well with the full-wave simulations. Lens performance parameters computed from each simulator are summarized in Table 1. Note that due to complex field interactions shown in Fig 1, field agreement beyond the lens diameter is more challenging, which leads to the sidelobe level difference. Because the compound lens doubles ray tracing implementation and iterative ray addition is added to the flowchart, the simulation time also doubles compared to the single-lens ray tracing reported in [11], but it is still much faster than full-wave simulation and maintains high accuracy.

REFERENCES

[1] A. Papathanasopoulos, J. Budhu, Y. Rahmat-Samii, R. E. Hodges, and D. F. Ruffatto, "3-d-printed shaped and material-optimized lenses for next-generation spaceborne wind scatterometer weather radars," *IEEE Transactions on Antennas and Propagation*, vol. 70, no. 5, pp. 3163–3172, 2022.

[2] S. Zhang, R. K. Arya, W. G. Whittow, D. Cadman, R. Mittra, and J. Vardaxoglou, "Ultra-wideband flat metamaterial GRIN lenses assisted with additive manufacturing technique," *IEEE Trans. Antennas Propag.*, pp. 1–1, 2020.

[3] N. Garcia and J. Chisum, "High-efficiency, wideband GRIN lenses with intrinsically matched unit-cells," *IEEE Trans. Antennas Propag.*, 2020. doi: 10.1109/TAP.2020.2990289.

[4] M. Albani, I. Gashi, A. Paraskevopoulos, and S. Maci, "Analysis and design of inhomogeneous dielectric lens antennas by using Geometrical Optics," in *2021 International Applied Computational Electromagnetics Society Symposium (ACES)*, 2021, pp. 1–4.

[5] P. F. Poyanco, JM. and E. Rajo-Iglesias, "Cost-effective wideband dielectric planar lens antenna for millimeter wave applications," *Scientific Reports*, vol. 12, 2022.

[6] W. Wang, N. Garcia, and J. Chisum, "The systematic design of non-commensurate impedance matching tapers for ultra wideband gradient-index (GRIN) lens antennas," *IEEE Transactions on Antennas and Propagation*, pp. 1–1, 2021 (Pre-print).

[7] N. Garcia, W. Wang, and J. Chisum, "Feed corrective lenslets for enhanced beamscan in flat lens antenna systems," vol. 30, no. 8, pp. 13 047–13 058, publisher: Optica Publishing Group. [Online]. Available: https://opg.optica.org/oe/abstract.cfm?uri=oe-30-8-13047

[8] N. C. Garcia and J. D. Chisum, "Compound grin fanbeam lens antenna with wideband wide-angle beam-scanning," *IEEE Transactions on Antennas and Propagation*, vol. 70, no. 9, pp. 7501–7512, 2022.

[9] J. Budhu and Y. Rahmat-Samii, "A novel and systematic approach to inhomogeneous dielectric lens design based on curved ray geometrical optics and particle swarm optimization," *IEEE Transactions on Antennas and Propagation*, vol. 67, no. 6, pp. 3657–3669, 2019.

[10] G. Gennarelli and G. Riccio, "A uniform asymptotic solution for the diffraction by a right-angled dielectric wedge," *IEEE Transactions on Antennas and Propagation*, vol. 59, no. 3, pp. 898–903, 2011.

[11] W. Wang and J. Chisum, "Hybrid geometrical optics and uniform asymptotic physical optics for rapid and accurate practical grin lens design," in *2022 IEEE/MTT-S International Microwave Symposium - IMS 2022*, 2022, pp. 20–23.